Determination of the acoustic phonon deformation potentials in diamond

V. Djurberg [ORCID],[*] S. Majdi [ORCID], N. Suntornwipat [ORCID], and J. Isberg [ORCID]

Division for Electricity, Department of Electrical Engineering, Uppsala University, Box 65, 751 03 Uppsala, Sweden

The interaction between acoustic phonons and electrons in diamond has been investigated by comparing state-of-the-art time-of-flight drift velocity measurements with Monte Carlo simulations. We use a multivariable anisotropic description of acoustic deformation potential scattering. The phonon-electron interaction is the limiting factor for the carrier mobility in ultrapure single crystal diamond. Hence, having a correct description is necessary for both device simulations and for predicting the maximum device performance. The experiments were performed at low temperature and using ultrapure diamond to minimize the influence of other scattering sources. The electronic valley polarization in diamond at low temperatures enables determination of both uniaxial and dilatation deformation potentials in the same experiment. The uniaxial and dilatation deformation potentials are found to be 18.5 ± 0.2 and -5.7 ± 0.3 eV, respectively.

I. INTRODUCTION

Diamond is an outstanding semiconductor material, with high thermal conductivity, breakdown voltage, electron and hole mobility and remarkable mechanical properties. This makes diamond an excellent candidate for, e.g., transistors for power electronics [1], single-photon sources [2], radiation detectors [3] and deep ultraviolet light-emitting diodes [4]. A limiting factor for many of these devices is the charge carrier mobility, which, for high quality single crystal chemical vapor deposited (CVD) diamond, is limited by phonon-electron interactions. These interactions depend on the electronic and mechanical properties of the diamond crystal and can be modelled using deformation potential theory [5].

The deformation potentials in diamond have not been investigated much compared to other group IV-semiconductors, such as Si and Ge [6–10], neither through experiments, e.g., cyclotron resonance, nor through *ab initio* simulations. Because of this, most charge transport and device simulations rely on a simple isotropic acoustic phonon deformation potential model, instead of a more accurate description with an anisotropic potential, as suggested by Herring and Vogt [5]. Due to the fact that the elastic anisotropy in diamond is large [11], the anisotropic approach to phonon scattering is much more appropriate for diamond. Hence, to achieve precise simulations of charge transport and to determine the deformation potentials, it is essential to take the phonon anisotropy into account.

In this work, we have measured electron drift velocity using the time-of-flight (ToF) method which has proved to be an extremely sensitive technique for measurements at very low carrier concentrations in highly resistive semiconductors [12–16]. The experimental data from the ToF measurements have been compared to Monte Carlo (MC) simulations, based on Herring and Vogt's work [5], to determine the deformation potentials in diamond. The results and the model can be used for an accurate description of electron transport in diamond.

II. EXPERIMENTAL TECHNIQUES

For this study, we selected a high purity single crystalline diamond sample synthesized by Element Six Ltd. The sample was grown along the [100] direction using the CVD method with a nitrogen impurity concentration < 0.05 ppb and a low surface roughness, R_a, below 5 nm. Titanium/aluminum/gold contacts were formed on both the top and bottom surface by means of physical vapor deposition. The top contact was made semitransparent through standard lithography and wet chemical etching. The ToF technique [17–19] was used to measure drift velocities for electrons through the sample in a weak electric field which was generated along the [100] direction by applying a negative bias voltage to the top contact. The electric field was applied in 50 μs pulses, in order to minimize polarization effects from charge build-up. The top surface of the sample was illuminated, through the semitransparent contact, by a quintupled 800 ps Nd:yttrium-aluminum-garnet laser with a repetition rate of 300 Hz and a wavelength of 213 nm. The laser pulses were applied synchronized with the electric pulses, as illustrated in Fig. 1. The sample is mounted on a sample holder in a vacuum cryostat using liquid helium as coolant. The experimental setup is shown in Fig. 1.

The photon energy of the laser (5.86 eV) is higher than the bandgap in diamond and creates electron-hole pairs near the illuminated surface. The penetration length is short, approximately 3 μm, compared to the thickness of the sample. The drift of free charges through the sample induces a current that can be measured at the contacts as described by the Shockley-Ramo theorem [20,21]. We measured the current

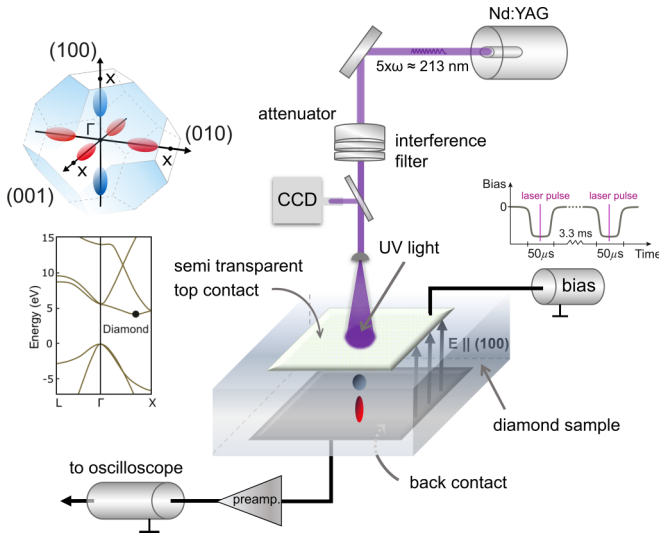*Corresponding author: viktor.djurberg@angstrom.uu.se

FIG. 1. Schematics of the time-of-flight (ToF) system used in the measurements, the cryostat is not shown. By applying a negative bias voltage at the illuminated contact, electrons drift through the sample, giving rise to a current that can be measured. The band structure and the first Brillouin zone of diamond with the conduction band minima (valleys) are depicted on the left.

for a set of temperatures and bias voltages and extracted the electron mobility from the transient current.

Diamond has a siliconlike band structure with six equivalent ellipsoidal energy minima in the conduction band. These are located on the {100} axes, as illustrated in Fig. 1. The effective mass in the valleys is described by the tensors:

$$\boldsymbol{m}_{\text{eff}\langle100\rangle} = \begin{pmatrix} m_l & 0 & 0 \\ 0 & m_t & 0 \\ 0 & 0 & m_t \end{pmatrix},$$

$$\boldsymbol{m}_{\text{eff}\langle010\rangle} = \begin{pmatrix} m_t & 0 & 0 \\ 0 & m_l & 0 \\ 0 & 0 & m_t \end{pmatrix},$$

$$\boldsymbol{m}_{\text{eff}\langle001\rangle} = \begin{pmatrix} m_t & 0 & 0 \\ 0 & m_t & 0 \\ 0 & 0 & m_l \end{pmatrix}, \tag{1}$$

where m_l (1.56 m_0) is the effective mass along the principal axis of the valley and m_t (0.28 m_0) is the effective mass in transversal directions. An electron will not scatter between valleys during drift unless it interact with a phonon of sufficient high energy and momentum. Because of the strong covalent bonds in diamond, these phonon energies are exceptionally high, starting at 140 meV [22]. Consequently, the scattering rate between valleys, at low temperatures and for sufficiently low electric fields, is negligible. For the electrons in the experiment and simulations in this article, the average energy of electrons is well below 140 meV as indicated in Fig. 2(b). Therefore, intervalley scattering can be neglected for the discussions in this article.

In addition, because the electrons do not change valley during transport, it is possible to observe valley polarization effects [19]. One such effect is that electrons in four of the six valleys perpendicular to the electric field along the [100] direction respond with effective mass m_t (fast electrons) and electrons in the other two valleys, parallel with the [100] respond with effective mass m_l (slow electrons). Due to this phenomenon, different electron velocities can be extracted from the two step current traces observed in Fig. 2(a) [23]. Another effect is that acoustic phonon scattering affects the electrons somewhat differently depending on which valley they occupy [5].

III. SIMULATIONS

We assume a parabolic energy band with all six ellipsoidal conduction band valleys explicitly included, see Supplemental Material [24]. The energy band model is a good approximation for low electric fields and temperatures. For high quality samples, electron-phonon scattering is the dominating scattering mechanism and all other mechanisms can be neglected [25]. The interaction is treated inelastically. Hence, the electrons change energy according to whether scattering was caused by emission or absorption of a phonon. The scattering probability that one electron will scatter from state $\boldsymbol{k}$ to state $\boldsymbol{k}'$ is [26]:

$$P_{\text{LA,TA}}^{a,e}(\boldsymbol{k}, \boldsymbol{k}') = \frac{\pi}{V \rho u_{\text{LA,TA}}} X_{\text{LA,TA}}(\Theta)q\left(N_{\text{LA,TA},q} + \frac{1}{2} \mp \frac{1}{2}\right)$$
$$\times \delta(\varepsilon(\boldsymbol{k}') - \varepsilon(\boldsymbol{k}) \mp \hbar u_{\text{LA,TA}}q), \tag{2}$$
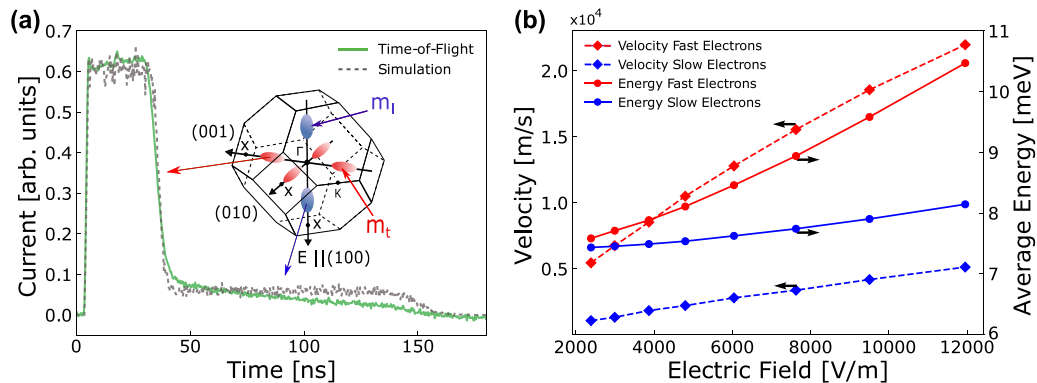

FIG. 2. (a) Example of current traces measured by the ToF technique at 80 K and an electric field of 7600 V/m, together with a MC simulation of the current trace, where the uniaxial and dilatation deformation potential have been assumed to be 18.5 eV and (−)5.7 eV, respectively. (b) Simulated electron average kinetic energy and velocity for different electric fields for a lattice temperature of 80 K.

where, u is the velocity of sound, ρ is the crystal density, V is the volume of the crystal, $\varepsilon(\boldsymbol{k})$ is the energy of state $\boldsymbol{k}$, and $N_{\mathrm{LA,TA},q}$ is the Bose-Einstein-distribution occupation number for a phonon with momentum q. In addition, the upper sign refers to absorption (a) and the lower sign to emission (e) of a phonon. LA stands for longitudinal acoustic phonon scat-

tering and TA for transversal acoustic phonon scattering. The anisotropy of the transversal phonon scattering factor $X_{\mathrm{TA}}(\theta)$ and longitudinal phonon scattering factor $X_{\mathrm{LA}}(\theta)$ is expressed through the dilatation and uniaxial deformation potentials, Ξ_d and Ξ_u, and θ, is the angle between the phonon wave vector and the principal axis of the valley [5]:

$$X_{\mathrm{LA}}(\theta) = \frac{(\Xi_d + \cos^2\theta\,\Xi_u)^2}{c_{12} + 2c_{44} + \frac{3}{5}c^*}\left[1 - \frac{c^*(0.15 - 1.5\cos^2\theta + 1.75\cos^4\theta)}{c_{12} + 2c_{44} + \frac{3}{5}c^*}\right],\tag{3}$$

$$X_{\mathrm{TA}}(\theta) = \Xi_u^2\cos^2\theta\sin^2\theta\left[\frac{3}{c_{44} + \frac{1}{3}c^*} - \frac{2}{c_{44} + \frac{1}{2}c^*} + 6\cos^2\theta\left(\frac{1}{c_{44} + \frac{1}{2}c^*} - \frac{1}{c_{44} + \frac{1}{3}c^*}\right)\right].\tag{4}$$

Here, c_{ij} are the elastic constants for diamond and $c^* = c_{11} - c_{12} - 2c_{44}$ is a measure of the elastic anisotropy in the crystal [11]. $X_{\mathrm{TA}}(\theta)$ includes the contributions from both modes of transversal phonons. Table I shows the basic parameters used in the simulations.

IV. RESULTS AND DISCUSSIONS

We measure ToF on the SC diamond sample and extract the transient time, for both fast and slow electrons, for temperatures of 40, 50, 60, 70, and 80 K and electric fields in the range 3000–10000 V/m. For each experimental temperature and electric field combination, we simulate over 150 transients using different values of the deformation potentials Ξ_u and Ξ_d in the range -24 to 24 eV. The MC simulations consists of 600 electrons, evenly distributed in the valleys drifting across a 490 μm thick diamond sample, to closely mimic the experimental situation. By comparing the simulated and experimental results for both fast and slow electrons it is possible find the combination of deformation potentials, Ξ_u and Ξ_d, that yield the correct transient times.

Figure 3 illustrates this for 50 K and an electric field set to 7600 V/m. The difference in transient time between the MC simulations and the experiment for both fast and slow electrons are plotted in the figure. The color represents the difference in transient time for the slow electrons and the black contour lines show the same for the fast electrons. Furthermore, the white curve in Fig. 3 represents the deformation potentials for which experimental and simulated transient time agree for slow electrons. Similarly, the zero deviation

contour line for fast electrons. The intersection between these two curves yield possible combinations of values for the deformation potentials. As can be seen in the figure, there are four choices of deformation potentials for which the transient time of the simulated fast and slow electrons agree with the experiments. These are approximately $\Xi_u = \pm 18.5$ eV, $\Xi_d = \mp 5.7$ eV and $\Xi_u = \pm 3.0$ eV, $\Xi_d = \pm 16.3$ eV.

We conclude that $\Xi_u = 18.5$ eV and $\Xi_d = -5.7$ eV is the correct combination by comparing our results with the deformation potentials from silicon and germanium, which have the same crystal structure as diamond [6]. Silicon also has a band structure very similar to diamond, with the conduction band minima located on the [100] axes as well. Both Si and Ge exhibit large positive uniaxial deformation potentials and much smaller (in absolute value) dilatation deformation potentials [6]. It can be assumed that diamond exhibits the same behaviour. In addition, density functional theory calculations of strained diamond indeed yield a positive value, approximately 20 eV for Ξ_u [30].

To achieve higher resolution, another set of simulations was performed in a narrow range around $\Xi_u = 18.5$ eV and $\Xi_d = -5.7$ eV with steps of 0.25 eV and 0.2 eV, respectively, see Fig. 4. There was no statistically significant change to

TABLE I. Parameters used in the Monte Carlo simulations.

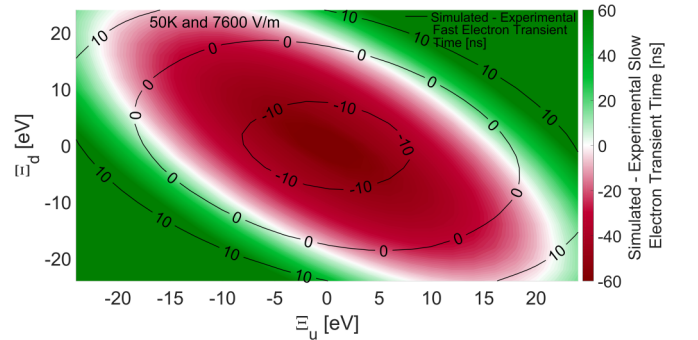| Parameter	Value	Source
Relative dielectric constant [1]	5.70	[27]
Crystal density [kg/m^3]	3.51×10^3	[27]
Longitudinal effective mass m_l [m_0]	1.56	[28]
Transverse effective mass m_t [m_0]	0.28	[28]
Velocity of sound u_{LA} [m/s]	17.52×10^3	[29]
Velocity of sound u_{TA} [m/s]	12.82×10^3	[29]
Elastic constants c_{11} [N/m^2]	10.79×10^{11}	[11]
Elastic constants c_{12} [N/m^2]	1.24×10^{11}	[11]
Elastic constants c_{44} [N/m^2]	5.78×10^{11}	[11]

FIG. 3. The deviation in transient time between the measurements and the simulations at a temperature of 50 K and an electric field of 7600 V/m, for different values of the deformation potentials. The color scale refers to the slow electrons and the black contour lines refer to fast electrons. The possible deformation potentials correspond to the four points where the deviation in transient time is zero for both fast and slow electrons.
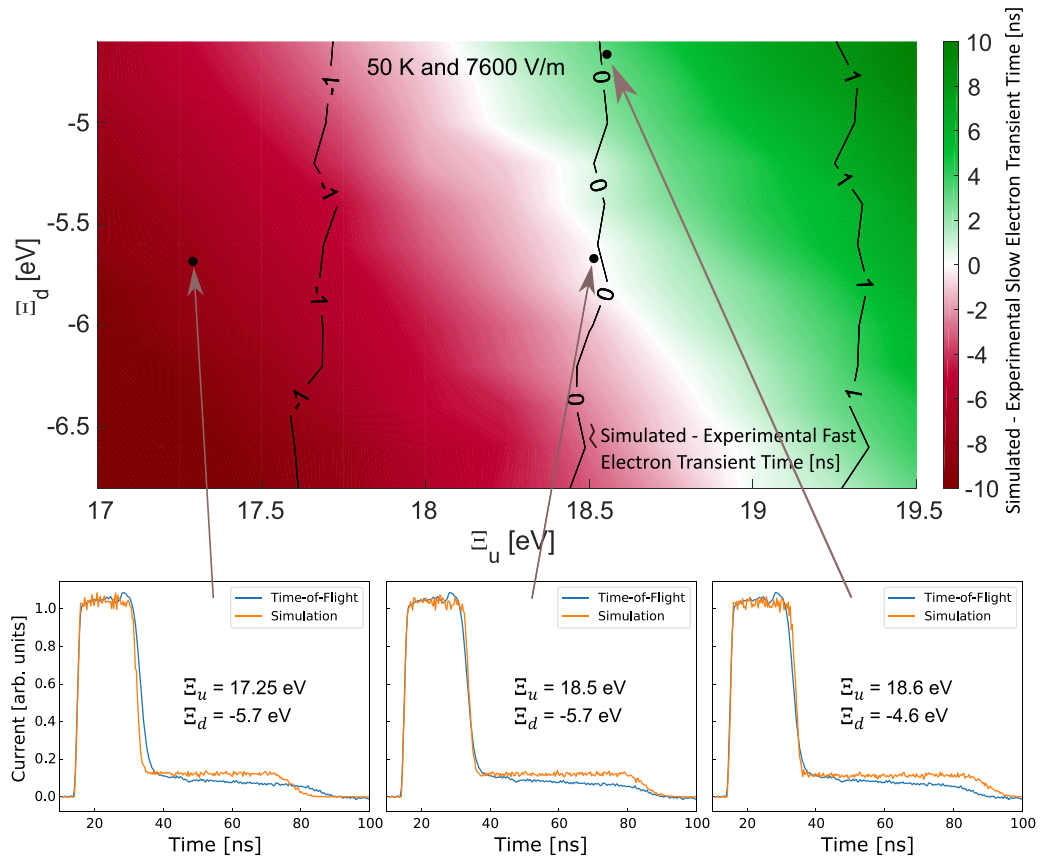
FIG. 4. Top: The deviation in transient time between the measurements and the simulations for 50 K and an electric field of 7600 V/m for different values of the deformation potentials. The slow electrons are shown with the color scale and fast electrons with the black contour lines. Below: Three examples of the simulated (orange) together with the measured currents (blue) with different deformation potentials, used to generate the above results. The arrows indicates the corresponding point in the above image the current traces generated.

the deformation potentials with a change in temperature. By averaging the results from all temperatures and electric fields, with the higher resolutions, the uniaxial and dilatation deformation potentials were determined to 18.5 ± 0.2 eV and -5.7 ± 0.3 eV, respectively. The remaining uncertainty originates from a small difference between the measured and simulated current traces (Fig. 4). This discrepancy arises from traps, inhomogeneity in the sample, and the fact that the electric field is not perfectly homogenous close to the sample edges. These deviations were noticeable at the lowest temperatures but are very small above 50 K.

V. CONCLUSIONS

We have measured the mobility of valley-polarized fast and slow electrons using the time of flight method. We compared the measurements with Monte Carlo simulations using an anisotropic multivariable description of the electron and acoustic phonon interaction. In doing so, we are able to determine the deformation potentials to $\Xi_u = 18.5 \pm 0.2$ eV

and $\Xi_d = -5.7 \pm 0.3$ eV. Anisotropic deformation potential theory has rarely been applied to diamond, compared to other group-IV-semiconductors. By providing a more precise description of the anisotropy in acoustic deformation potential scattering, our results can be used to gain a better understanding of electron transport and yield more reliable device simulations, e.g. for diamond electronic devices and radiation detectors.

[1] Circuits and applications, in *Power Electronics Device Applications of Diamond Semiconductors*, edited by S. Koizumi, H. Umezawa, J. Pernot, and M. Suzuki (Woodhead Publishing, Cambridge, 2018), Vol. 6, pp. 383–431.

[2] E. Neu and C. Becher, Diamond-based single-photon sources and their application in quantum key distribution, in *Quantum Information Processing with Diamond*, edited by S. Prawer and I. Aharonovich (Woodhead Publishing, Cambridge, 2014), Vol. 6, pp. 127–159.

[3] E. Bossini and N. Minafra, Diamond detectors for timing measurements in high energy physics, Front. Phys. **8**, 248 (2020).

[4] M. Dutta, F. A. M. Koeck, W. Li, R. J. Nemanich, and S. Chowdhury, High voltage diodes in diamond using (100)- and (111)- Substrates, IEEE Electron Device Lett. **38**, 600 (2017).

[5] C. Herring and E. Vogt, Transport and deformation-potential theory for many-valley semiconductors with anisotropic scattering, Phys. Rev. **101**, 944 (1956).

[6] M. V. Fischetti and S. E. Laux, Band Structure, deformation Potentials, and carrier mobility in strained Si, Ge, and SiGe alloys, J. Appl. Phys. **80**, 2234 (1996).

[7] F. Szmulowicz and F. L. Madarasz, Full-Boltzmann-equation solutions of the acoustic-phonon-limited conductivity and hall mobilities for P -Type silicon and germanium, Phys. Rev. B **27**, 6279 (1983).

[8] Y. Sun, S. E. Thompson, and T. Nishida, Physics of strain effects in semiconductors and metal-oxide-semiconductor field-effect transistors, J. Appl. Phys. **101**, 104503 (2007).

[9] R. Oberhuber, G. Zandler, and P. Vogl, Subband structure and mobility of two-dimensional holes in strained Si/SiGe MOSFET's, Phys. Rev. B **58**, 9941 (1998).

[10] E. Pop, R. W. Dutton, and K. E. Goodson, Analytic band Monte Carlo model for electron transport in Si including acoustic and optical phonon dispersion, J. Appl. Phys. **96**, 4998 (2004).

[11] H. J. McSkimin and P. Andreatch, Elastic moduli of diamond as a function of pressure and temperature, J. Appl. Phys. **43**, 2944 (1972).

[12] J. Isberg, J. Hammersberg, E. Johansson, T. Wikström, D. J. Twitchen, A. J. Whitehead, S. E. Coe, and G. A. Scarsbrook, High carrier mobility in single-crystal plasma-deposited diamond, Science **297**, 1670 (2002).

[13] L. Reggiani, S. Bosi, C. Canali, F. Nava, and S. F. Kozlov, Hole-Drift velocity in natural diamond, Phys. Rev. B **23**, 3050 (1981).

[14] S. Majdi, V. Djurberg, N. Suntornwipat, M. Gabrysch, and J. Isberg, Carrier scattering Mechanisms: identification via the scaling properties of the Boltzmann transport equation, Adv. Theory Simul. **4**, 2000103 (2021).

[15] L. S. Pan, D. R. Kania, P. Pianetta, J. W. Ager, M. I. Landstrass, and S. Han, Temperature dependent mobility in Single-crystal and chemical vapor-deposited diamond, J. Appl. Phys. **73**, 2888 (1993).

[16] N. Suntornwipat, M. Gabrysch, S. Majdi, D. J. Twitchen, and J. Isberg, Magnetotransport study of valley-polarized electrons in synthetic diamond, Phys. Rev. B **94**, 035408 (2016).

[17] M. Gabrysch, S. Majdi, D. J. Twitchen, and J. Isberg, Electron and hole drift velocity in chemical vapor deposition diamond, J. Appl. Phys. **109**, 063719 (2011).

[18] S. Majdi, K. K. Kovi, J. Hammersberg, and J. Isberg, Hole transport in single crystal synthetic diamond at low temperatures, Appl. Phys. Lett. **102**, 152113 (2013).

[19] J. Isberg, M. Gabrysch, J. Hammersberg, S. Majdi, K. K. Kovi, and D. J. Twitchen, Generation, transport and detection of valley-polarized electrons in diamond, Nat. Mater. **12**, 760 (2013).

[20] W. Shockley, Currents to conductors induced by a moving point charge, J. Appl. Phys. **9**, 635 (1938).

[21] S. Ramo, Currents induced by electron motion, Proc, IRE **27**, 584 (1939).

[22] F. Nava, C. Canali, C. Jacoboni, L. Reggiani, and S. F. Kozlov, Electron effective masses and lattice scattering in natural diamond, Solid State Commun. **33**, 475 (1980).

[23] J. Isberg, J. Hammersberg, D. J. Twitchen, and A. J. Whitehead, Single crystal diamond for electronic applications, Diam. Relat. Mater. **13**, 320 (2004).

[24] See Supplemental Material at http://link.aps.org/supplemental/10.1103/PhysRevB.106.045205 for a description of the Monte Carlo code used for simulations.

[25] K. Konishi, I. Akimoto, H. Matsuoka, V. Djurberg, S. Majdi, J. Isberg, and N. Naka, Low-Temperature mobility-lifetime product in synthetic diamond, Appl. Phys. Lett. **117**, 212102 (2020).

[26] C. Jacoboni and L. Reggiani, The Monte Carlo method for the solution of charge transport in semiconductors with applications to covalent materials, Rev. Mod. Phys. **55**, 645 (1983).

[27] *Semiconductors—Basic Data*, edited by O. Madelung (Springer, Berlin, 1996).

[28] N. Naka, K. Fukai, Y. Handa, and I. Akimoto, Direct measurement via cyclotron resonance of the carrier effective masses in pristine diamond, Phys. Rev. B **88**, 035205 (2013).

[29] S. Koizumi, C. E. Nebel, and M. Nesladek, *Physics and Applications of CVD Diamond* (Wiley-VCH, Weinheim, 2008).

[30] C. Dang *et al.*, Achieving large uniform tensile elasticity in microfabricated diamond, Science **371**, 76 (2021).